ADVANCED THERAPEUTICS
www.advtherap.com

Hydrogel Microsphere Encapsulation Enhances the Flow Properties of Monoclonal Antibody Crystal Formulations

*Jeremy M. Schieferstein, Paul Reichert, Chakravarthy N. Narasimhan, Xiaoyu Yang, and Patrick S. Doyle**

Monoclonal antibodies are therapeutic molecules known for their high specificity and versatility in the treatment of cancer and autoimmune disorders, but dosage forms are typically limited to low concentrations and large fluid volumes due to formulation challenges. Hydrogel microsphere formulations offer a route to quicker, patient-friendly dosing regimens for monoclonal antibodies with high loading and favorable flow properties needed for injection through a narrow syringe needle under moderate applied force. Crystals of an intact monoclonal antibody are prepared as a concentrated suspension (>300 mg mL^{-1}) which is then encapsulated within hydrogel microspheres with diameters as small as 30 µm. The hydrogel microspheres contain up to 56 wt% (dry basis) monoclonal antibody and release within 4 days under in vitro dissolution conditions. The hydrogel microspheres are concentrated into densely packed suspensions containing up to 300 mg mL^{-1} monoclonal antibody to evaluate their flow. These hydrogel formulations shear-thin and have lower viscosity when compared to both liquid and suspended crystal forms of the monoclonal antibody, demonstrating the potential of hydrogel microsphere encapsulants as a carrier which can mask undesirable flow properties of concentrated antibody therapeutics.

1. Introduction

Monoclonal antibodies (mAbs) are therapeutics known for their high specificity and versatility for the treatment of cancer and autoimmune disorders.[1,2] Typically, mAbs are administered every few weeks via intravenous infusion in clinics with each administration requiring a few hours of time and the aid of a healthcare professional. The development of suitable formulations for subcutaneous injection of monoclonal antibodies is a significant therapeutic goal toward greater patient convenience and self-administration. For the subcutaneous route, these formulations would require a high concentration of mAbs (≫100 mg mL^{-1}) to meet volume requirements (<1.5 mL) for injection,[3] although a formulation with such concentrations introduces additional challenges. At high concentrations, mAbs self-associate and form aggregates in solution, which manifests as high viscosity.[4] Proactive strategies to engineer the viscosity of the formulation, such as changes in buffer conditions, addition of thinning excipients, or minor modifications to the mAb may be considered throughout development to avoid unacceptably high injection forces for administration.[5] High concentration antibody solutions are also susceptible to accelerated protein degradation due to aggregation, which potentially impacts protein activity, pharmacokinetics, and safety.[6]

Small molecule drugs are commonly prepared in solid forms (e.g., amorphous solid dispersions, crystals) to impart the formulation with certain flow properties, greater solubility, enhanced stability, and tunable release properties. The crystalline form of proteins, while traditionally used for purification and structural characterization, can analogously be utilized to stabilize high concentration formulations of mAbs or other proteins.[7] Crystals themselves are naturally densely packed with stable and folded protein at very high concentration (potentially >500 mg mL^{-1}).[8] Further, some suspensions of protein crystals exhibit lower viscosities when compared to protein solutions of equivalent concentrations.[9] Due to difficulties in developing protein crystal formulations (e.g., finding safe, suitable crystallization and stabilization conditions; scale-up of crystallization batch size), there has been limited commercial success outside of crystalline insulin, where crystals impart the formulations with long-lasting release.[10] Consequently, there is significant room for development and innovation in this area.

Hydrogel materials are often studied as carriers for drug delivery due to their high water content, softness, and biocompatibility.[11,12] Hydrogels can be produced with a variety of chemistries and microstructures,[13–16] which enable design of hydrogels with diverse surface affinity and tunable drug release kinetics (e.g., fast release via hydrogel matrix degradation, slow release via diffusion).[17,18] Prior works have exploited hydrogels for delivery of small molecule drugs in either the aqueous or crystalline form,[19–21] and proteins in the aqueous form.[22,23] These hydrogels are either formed in situ after injection by triggered gelation (e.g., pH, temperature), or formed beforehand

Dr. J. M. Schieferstein, Prof. P. S. Doyle
Department of Chemical Engineering
Massachusetts Institute of Technology
Cambridge, MA 02142
E-mail: pdoyle@mit.edu
P. Reichert, Dr. C. N. Narasimhan, Dr. X. Yang
Merck Research Laboratories
Kenilworth, NJ 07033

DOI: 10.1002/adtp.202000216

© 2021 Wiley-VCH GmbH

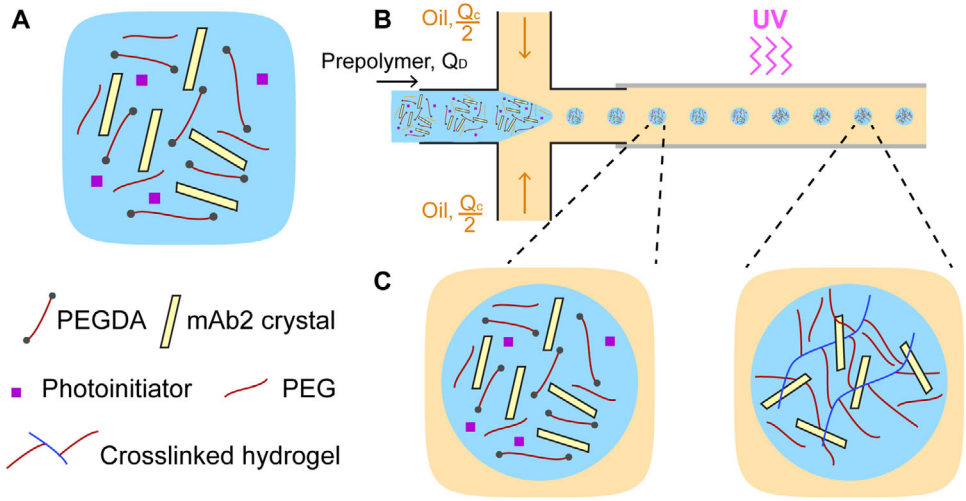

Figure 1. Schematic of formulation strategy for hydrogel/crystal microspheres. A) Hydrogel prepolymer was prepared by direct mixing of a concentrated suspension of mAb2 crystals in a PEG buffer, PEGDA, and photoinitiator. B) Hydrogel prepolymer droplets produced by using a microfluidic crossjunction; each droplet crosslinked by exposure to UV light. C) Crystals are well suspended within prepolymer droplets before crosslinking. After UV exposure, micron-scale crystals are trapped within the nanoporous matrix of the crosslinked microsphere. Schematic not to scale.

for use as an oral formulation or implantable depot. Hydrogels can also be prepared as microsphere suspensions which exhibit lower viscosities when injected through a needle[24,25] (i.e., high shear) and reach high volume fractions due to their ability to de-swell and deform when densely packed.[26] These properties make microsphere suspensions an interesting carrier to explore for a high concentration, low viscosity formulation.

Here, we report a hydrogel/crystal microsphere formulation of a monoclonal antibody "mAb2". mAb2 was prepared as a concentrated suspension of crystals (>300 mg mL^{-1}) which was then encapsulated within hydrogel microspheres. The hydrogel microspheres were characterized to validate mAb2 crystallinity, mAb2 loading, and encapsulation efficiency. Further, in vitro dissolution experiments were conducted to demonstrate drug release from the hydrogel/crystal formulation. The functional integrity of mAb2 dissolved from hydrogel particles was characterized using chromatography and an enzyme-linked immunosorbent assay (ELISA) binding bioassay. Finally, the flow curves of concentrated hydrogel/crystal microsphere suspensions demonstrated the improved flow properties of this formulation when compared to other forms of concentrated mAb2.

2. Results and Discussion

2.1. Production of Hydrogel/Crystal Microspheres

The hydrogel prepolymer was designed to polymerize under ultraviolet (UV) irradiation and to stabilize suspended mAb2 crystals (**Figure 1**A). A concentrated suspension of mAb2 crystals in a 10% w/v poly(ethylene glycol) (PEG, MW 3350 Da), 50 mM 4-(2-hydroxyethyl)-1-piperazineethanesulfonic acid (HEPES), pH 7.0, stabilization buffer was first prepared (Figure S1, Supporting Information), and then mixed with poly(ethylene glycol) diacrylate (PEGDA, M_W 700), a molecule which forms biocompatible hydrogels with predictable mesh size and degradability.[27,28] Since mAb2 crystals were prepared and stabilized in a concentrated PEG buffer, it was anticipated that formulation in the presence of PEGDA would not significantly disrupt mAb2 crystallinity throughout processing. The amount of PEGDA and photoinitiator (Darocur 1173) were optimized (10% and 1.5% v/v respectively) such that PEGDA rapidly polymerized (<60 s) when exposed to UV, and that photoinitiator was fully soluble in the blend. The balance of the prepolymer blend (88.5% v/v) was up to 330 mg mL^{-1} mAb2 crystals in their stabilization buffer. The PEG component of the buffer both stabilizes the mAb2 crystals and induces the formation of interconnected pores within the polymerized hydrogel, which increases diffusion rates through the hydrogel.[29,30]

A simple microfluidic crossjunction and a ultraviolet light-emitting diode (UV LED)[31] were utilized to produce hydrogel/crystal microspheres as small as 30 µm in diameter (Figure 1, and Figure S2, Supporting Information).The size and dispersity of hydrogel particles were influenced by flow rates of the mineral oil and prepolymer, Q_C and Q_D (respectively), their viscosities μ_C and μ_D, and the interfacial tension. The flow rates (Q_c, Q_D) are the most straightforward levers of control for generating a hydrogel product with a specific size. The viscosity of the dispersed phase is limited by its mAb2 load. Different oils and surfactants can be utilized to adjust viscosity and interfacial tension to grant greater control over droplet production. Microspheres were continuously produced at a rate Q_D of 0.1–1 µL min^{-1} in an immiscible carrier fluid (mineral oil). Microsphere loading C_{load} was controlled by mixing a certain volume of concentrated mAb2 crystals into the prepolymer, and defined as

$$C_{load} = \frac{v_m C_m}{v_t} \quad (1)$$

where v_m was the volume of mAb2 crystal suspension of concentration C_m, and v_t was the final volume of mixed prepolymer. Microspheres with 50 µm in diameter (CV = 0.04) were used for characterization at 50 and 100 mg mL^{-1} mAb2 loadings.

© 2021 Wiley-VCH GmbH

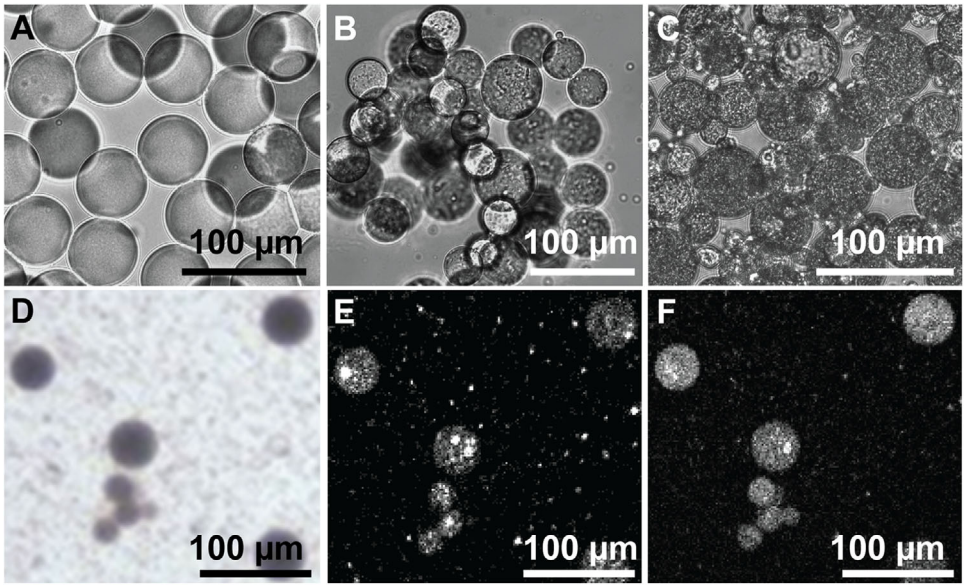

Figure 2. Microscopic imaging of hydrogel microspheres samples loaded with A) 0 mg mL^{-1}, B) 100 mg mL^{-1}, or C) 300 mg mL^{-1} of mAb2 crystals. The same sample of microspheres containing 200 mg mL^{-1} of mAb2 crystals were imaged in D) bright field, E) second harmonic generation (SHG), and F) ultraviolet two-photon excited fluorescence (UV-TPEF).

High concentration suspensions of mAb2 crystals exhibit high viscosities (≫0.1 Pa s), and likewise, prepolymer solutions containing high concentrations of mAb2 crystals were also very viscous. For prepolymers with >200 mg mL^{-1} mAb2, the microfluidic device yielded populations of smaller microspheres with higher polydispersity (30 µm diameter, CV = 0.3). After production, microspheres were separated from the mineral oil, washed with fresh PEG buffer, and were stored and characterized as a hydrated suspension.

With this device, up to 18 mg h^{-1} of crystalline mAb2 can be processed into hydrogel microspheres. For example, to produce a 1.5 mL hydrogel microsphere dosage containing 450 mg of mAb2 the device must be run for 25 h. To reach scale, the process would have to be adapted to high-throughput microparticle production technologies which typically operate in parallel with hundreds of droplet-producing nozzles.[32,33] Companies that specialize in microfluidics report high-throughput systems that produce up to 1 ton of particles per month.[34]

2.2. Characterization of Hydrogel/Crystal Microspheres

Hydrogel/crystal microspheres were spherical in shape and opaque with an apparently rough texture (**Figure 2**). The features of small, needle-shaped mAb2 crystals could be distinguished within the microspheres under high magnification (Figure S3, Supporting Information). Second harmonic generation (SHG) microscopy confirmed the presence of chiral crystals, and ultraviolet two-photon emission fluorescence (UV-TPEF) microscopy confirmed the presence of mAb2, which together confirmed that the hydrogel particles were packed with mAb2 crystals. The crystals were encapsulated and constrained within the hydrogel mesh, and they remained localized within hydrogels throughout polymerization and wash procedures without leakage. Further, the porous hydrogel enabled sufficient solvent access of PEG buffer to mAb2 crystals such that encapsulated material did not prematurely lose crystallinity or dissolve.

Microsphere loading of mAb2 in hydrogels was measured through thermogravimetric analysis. Control mAb2 decomposed over the temperature range 150–350 °C, and a residual mass was present at 500 °C. A PEG hydrogel control sample decomposed sharply between temperatures of 350–425 °C, and was fully decomposed at 500 °C. Details of the data calculations and analysis are included in the Supporting Information (Figure S4, Supporting Information). Microspheres prepared with 50, 100, 200, and 300 mg mL^{-1} of mAb2 were determined to have loadings of 27.5, 38.3, 51.6, and 56.1 wt% respectively. 100% encapsulation was achieved for microsphere loadings <200 mg mL^{-1}, and 89% at 300 mg mL^{-1} loading (**Figure 3** and Table S1, Supporting Information). We attribute the high encapsulation efficiency to the oil-in-water method used to sequester all crystalline material into droplets. Further, high loadings indicated that the mesh of the hydrogel was densely filled with mAb2. The drop-off in encapsulation efficiency at 300 mg mL^{-1} was attributed to pipetting inefficiencies while handling and loading the prepolymer into syringes due to high viscosity and paste-like quality at high concentration of crystals.

2.3. In vitro Release of mAb2 from Hydrogel Microspheres

Hydrogel particles loaded with mAb2 crystals were immersed in phosphate buffered saline (PBS). mAb2 dissolved from the crystals and released by diffusion through the porous polymer matrix, and the release rate was influenced by factors such as size of the antibody, polymer molecular weight, concentration of porogens, crosslink density, and size of the hydrogel particle.[35,36] Within minutes, the appearance of the hydrogel particles changed from

© 2021 Wiley-VCH GmbH

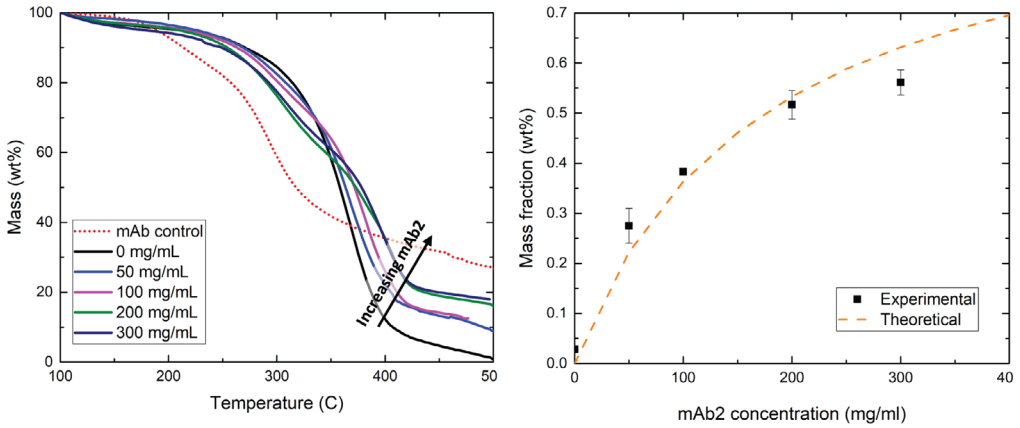

Figure 3. Thermogravimetric analysis of hydrogels loaded with mAb2 crystals. A) Decomposition profiles of samples at microsphere loadings from 0–300 mg mL^{-1}. B) Comparison of measured and theoretical values of mass for each hydrogel sample. Standard deviations represented as error bars for three replicate samples.

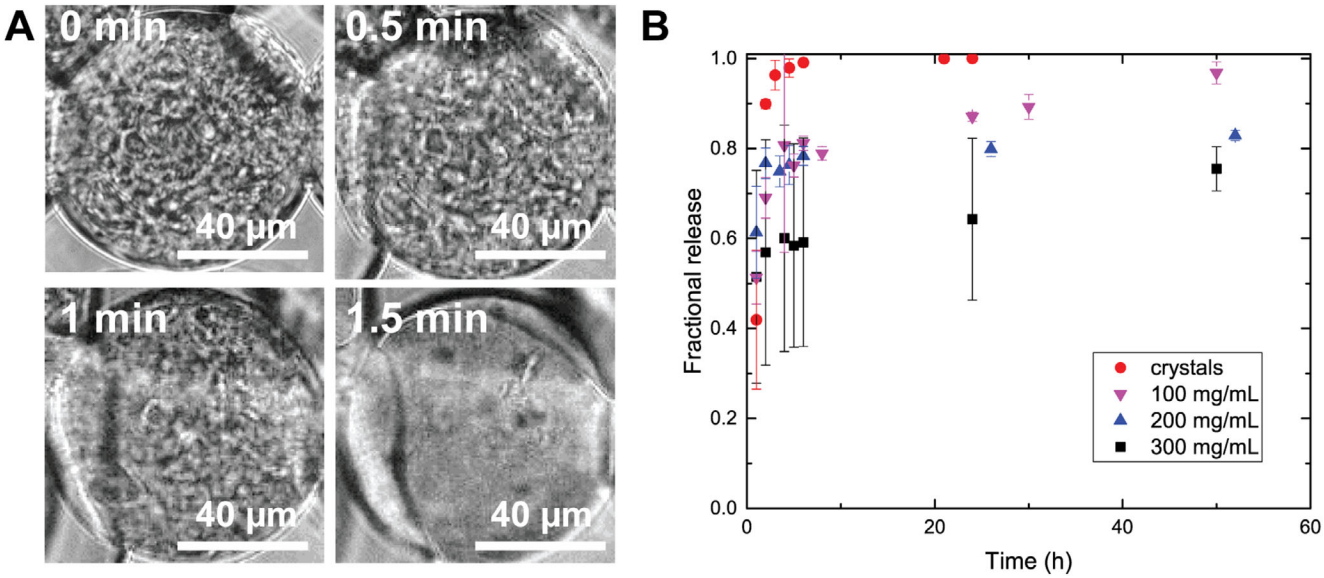

Figure 4. In vitro release from hydrogels loaded with mAb2 crystals. A) Time-lapse imaging of crystal dissolution. The observed texture of the hydrogels evolves over 1.5 min until the hydrogels are no longer opaque. B) Fractional release profiles from hydrogel particles loaded with 100, 200, or 300 mg mL^{-1} of mAb2. Standard deviations represented as error bars for three replicate samples.

opaque to transparent and were no longer birefringent under crossed polarizers (**Figure 4**A, Videos S1 and S2, Supporting Information), indicating that the embedded crystals had dissolved. Interestingly, the dissolution profile indicates that after an initial burst release, mAb2 slowly released from hydrogels over for several hours to several days, with a slight dependence on the concentration of mAb2 encapsulated (Figure 4B). Notably, mAb2 release did not reach 100% for all hydrogel preparations. This indicates that some mAb2 was unable to easily leave hydrogel particles, possibly because some mAb2 was entrapped within low porosity regions of a hydrogel particle which would release over the course of weeks-to-months as noted in prior studies of hydrogel release.[17,37]

We attribute the burst release to heterogeneous crosslinking along the radius of particles due to oxygen-inhibition of free radical polymerization[38] and mild swelling of the hydrogels upon transfer to dissolution media[39]. Further, the observation of rapid crystal dissolution and prolonged release indicates a two-step mechanism for the release of mAb2. First, the dissolution media rapidly penetrates the hydrogel particle, and dilutes the stabilizing PEG buffer surrounding and within the crystals, leading to mAb2 crystal dissolution. The large mAb2 molecules ($D_h \approx 11.1$ nm by dynamic light scattering) then diffuse through the porous hydrogel matrix over several days. We suggest that the slower observed dissolution at high mAb2 concentrations arose from a local increase in viscosity within the hydrogel microspheres upon immersion and the dissolution of mAb2 crystals, which led to a suppression of the effective diffusion coefficient,[40] although a complete investigation of release kinetics would be required to elucidate this phenomenon.

© 2021 Wiley-VCH GmbH

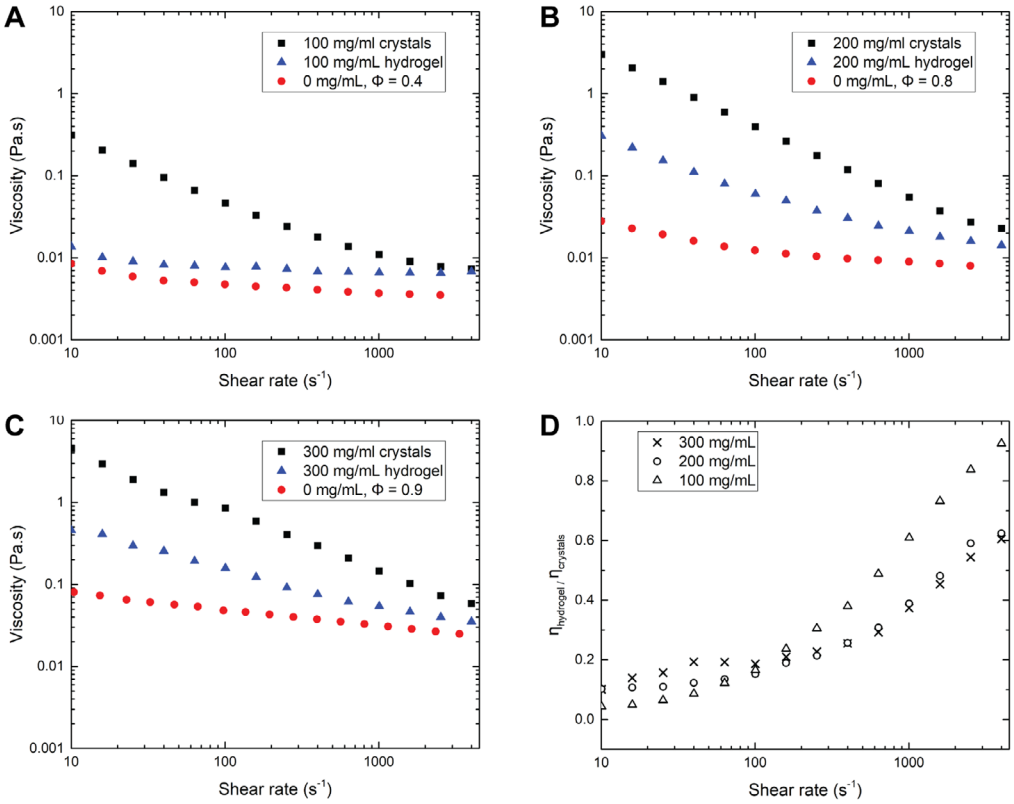

Figure 5. Flow curves for mAb2 samples in the form of a suspension of crystals (black), hydrogel encapsulated crystals (blue), and a comparable volume fraction of hydrogels without mAb2 loading (red). Viscosity was plotted against shear rate for formulated mAb2 concentrations of A) 100 mg mL^{-1}, B) 200 mg mL^{-1}, and C) 300 mg mL^{-1} suspended in a HEPES buffer at pH 7.0 containing 10% PEG. D) Viscosity reduction ratio for encapsulated crystals versus suspended crystals at each formulated load.

2.4. Flow Curves of Concentrated Hydrogel & Crystal Suspensions

To evaluate how hydrogel/mAb2 crystal microspheres would perform in an injection, high loading microspheres were prepared as dense particle suspensions and their flow curves were analyzed. Nominal particle volume fraction of hydrogel microspheres was defined as

$$\Phi = \frac{v_t}{v_f} \tag{2}$$

where v_t is the volume of prepolymer converted into microspheres, and v_f is the final volume of the sample for rheometry. The formulated hydrogel load was defined as

$$C_{form} = C_{load}\,\Phi \tag{3}$$

where C_{load} was the microsphere loading and Φ is the nominal volume fraction of spheres (Table S2, Supporting Information). The nominal volume fraction of microspheres in each suspension was tuned to achieve a final formulated load to compare the hydrogel form to equivalent mAb2 dosages in either the crystal suspension form or concentrated solution form. For example, to prepare the most concentrated hydrogel formulation studied here of 300 mg mL^{-1}, microspheres were prepared with a microsphere loading of 333 mg mL^{-1} mAb2 and centrifuged to a nominal particle volume fraction of 0.9. The rheometer gap size was set to 0.25 mm to approximate the inner diameter of a 26-gauge needle to optimize sample while reducing the potential flow effects of confinement. The gap size was at least 5× larger than the mean particle diameter. In the case of a subcutaneous injection where 1 mL is delivered in ≈10 s, the wall shear rate inside a 26-gauge needle is >57 000 s^{-1}. Due to sample and instrumentation limitations, flow curves were measured with a maximum shear rate of 4000 s^{-1}. At this limit, hydrogel samples approach a viscosity plateau, and previous reports show that the viscosity of suspensions of soft particles often plateau and typically do not shear thicken.[26] As a comparison, concentrated mAb2 solutions, mAb2 crystal suspensions, and unloaded hydrogels were analyzed using the same experimental setup (**Figure 5**;FigureS5, Supporting Information). Hydrogel suspensions may experience wall slip under shear conditions on the rheometer, which would reduce the measured viscosity; however, well above the yield stress, slip is negligible compared to the bulk flow, and the measured viscosity should approach the true viscosity at a given shear rate.[41] We confirmed this behavior in PEGDA hydrogel samples at low shear rates (Figure S5D, Supporting Information), thus we limited our interpretation of viscosity to data collected in the high shear regime (>100 s^{-1}).

© 2021 Wiley-VCH GmbH

Solutions of mAb2 at 100 and 200 mg mL^{-1} had a constant, low viscosity under shear. At 300 mg mL^{-1} mAb2 solutions exhibited shear thinning and high viscosity (>0.6 mPa s) (Figure S5B, Supporting Information). This behavior agrees with prior studies of antibody solutions that observed reversible self-association under shear which was attributed to mAb–mAb interactions and aggregation at high concentrations.[42,43] mAb2 crystal suspensions shear thinned at all concentrations measured, and at 200 and 300 mg mL^{-1} had equivalent or lower viscosity than the corresponding solution form at a shear rate of 4000 s^{-1}. Unloaded hydrogel particle suspensions also shear thinned and plateaued at a viscosity that depended on the particle volume fraction (Figure S5C, Supporting Information). Hydrogels containing mAb2 crystals shear thinned, and interestingly their behavior was bounded by an equivalent volume fraction of unloaded hydrogel particles and an equivalently concentrated suspension of crystals across all shear rates (Figure 5A–C). This behavior was consistent for 100, 200, and 300 mg mL^{-1} formulated loads. Notably, the measured viscosity of the 300 mg mL^{-1} formulation under shear was <0.035 Pa s, an indication of potential suitability as an injectable formulation. In a qualitative injectability test, a hydrogel sample with 300 mg mL^{-1} formulated load was successfully ejected from a 26-gauge needle by hand without difficulty (Video S3, Supporting Information).

To estimate of the required force to inject a shear thinning 300 mg mL^{-1} mAb2-laden hydrogel suspension, the high shear rate flow curve data (>100 s^{-1}) was fit as a power-law fluid to determine characteristic flow consistency index and flow behavior index. The pressure and force was calculated using a hydraulics equation to account for the non-Newtonian behavior of a power-law fluid:[44,45] for a 26, 27, or 30 gauge needle with a 1 mL syringe, injection would require 5.3, 9.2, or 19 N respectively (further details in Supporting Information). When compared to a recent study of maximum applicable forces by humans during injection, the 300 mg mL^{-1} hydrogel microsphere suspension would be considered easy to inject through a 26 or 27 gauge needle, and would require a "considerable effort" to inject through a 30 gauge needle.[46]

We rationalize that the improved flow behavior of the crystal-laden microspheres arises from three effects: 1) the hydrogel cloaks mAb–mAb interactions of embedded crystals, 2) the spherical microsphere shape minimizes surface area-to-volume ratio of particles such that exposed (surface) mAb crystals have a smaller contribution to viscosity; and 3) the hydrogel formulation is soft and deformable, resulting in enhanced flow behavior under shear. At low concentrations, the cloaking effect is most pronounced as the microspheres contain a low volume of crystals, and the flow properties of the hydrogel particle dominates. At high concentrations, a large volume of the hydrogel is occupied by mAb2 crystal, and thus we expect the hydrogels to behave effectively as a “spherical crystal” with lower viscosity than an equivalent mass of mAb2 as a crystal suspension. In this report, all hydrogel formulations resulted in a decrease in viscosity relative to crystal suspensions (Figure 5D). Notably, at a shear rate of 100 s^{-1} the 300 mg mL^{-1} hydrogel formulation had a 5.2-fold decrease in viscosity compared to the crystal suspension, and over a 50-fold decrease in viscosity compared to the concentrated mAb2 solution.

2.5. Assessment of mAb2 Stability and Functionality

2.5.1. Ultra-Performance Size Exclusion Chromatography(UPSEC) Data

mAb2 dissolved from hydrogel microparticles was analyzed by ultra-performance size exclusion chromatography to evaluate aggregation induced by formulation in hydrogels (Figure S6, Supporting Information). >93% of dissolved mAb2 remained monomeric, indicating that mAb2 was not significantly aggregating after hydrogel processing (crystallization, encapsulation, dissolution, and subsequent handling).

2.5.2. Bioassay data

Samples from mAb2 crystals encapsulated in hydrogel microparticles immersed in normal saline phosphate buffer (PBS) and a control mAb2 sample (control) before crystallization were analyzed in an ELISA binding assay.[47] The geometric mean of relative potency from multiple replicates ($N = 3$) of the same sample is reported with geometric standard deviation (%GSD) and 95% confidence interval. The potency of mAb2 samples in a competitive binding ELISA is shown in Table S5, Supporting Information. These results demonstrated the overall process (crystallization, encapsulation, dissolution, and subsequent handling) did not negatively affect the mAb2 in the competitive binding functionality within the error of the ELISA binding assay.

We anticipate that the stability of the drug substance can be further optimized in hydrogel microparticle formulations in future studies of encapsulation with more bioorthogonal hydrogel materials and gelation methods.

2.6. Conclusions

In summary, we produced hydrogel microspheres containing monoclonal antibody crystals with high loadings and low viscosity. We demonstrated that maintaining these formulations in a PEG-rich buffer preserved the crystallinity of the mAb2 cargo, and that upon transfer to dissolution conditions, crystals dissolved and mAb2 released from the hydrogel matrix. When hydrogel/crystal microspheres were formulated as dense suspensions at high formulated loadings, they shear thinned and had lower viscosities than equivalent concentrations of mAb2 in crystal suspensions, demonstrating that crystal-loaded hydrogel microspheres may help overcome flowability issues for high concentration therapeutic dosages. The encapsulation process induced a small degree of aggregation, but the potency of mAb2 was unaffected. While PEGDA was used to synthesize hydrogel microspheres in this study, the approach may be applied and optimized in other hydrogel systems to further consider the release properties, performance, biocompatibility, and fate of the hydrogel carrier.[48,49] Further, crystallinity of mAb throughout processing may imply that the mAb was not impacted by gelation and the hydrogel chemistry, but a molecular-level analysis of compatibility between the chemistry of the hydrogel and mAb must also be conducted before consideration of such a

© 2021 Wiley-VCH GmbH

formulation for clinical use, including (but not limited to) aggregation, denaturation, bioorthogonality, and potency.

3. Experimental Section

Purified, humanized monoclonal antibody (mAb2) was provided by Merck. Mineral oil ("light mineral oil", M3516), poly(ethylene glycol) diacrylate (PEGDA, molecular weight 700), 2-hydroxy-2-methylpropiophenone (Darocur 1173), sorbitane monooleate (Span 80), caffeine, and 4-(2-hydroxyethyl)-1-piperazineethanesulfonic acid (HEPES) were from Sigma. Poly(ethylene glycol) (PEG, molecular weight 3350) was from Hampton Research.

For crystallization, "PEG buffer" was prepared as a 10% w/v PEG solution in 50 mM HEPES, pH 7.0. "Caffeine buffer" was prepared as a 2.5% w/v caffeine solution in 20 mM L-His, pH 5.4. mAb2 was prepared at 40 mg mL^{-1} in 20 mM L-His, pH 5.4. Solutions were prepared with distilled water and were sterile filtered with a 0.22 micron SUPOR filter (Acrodisc).

Crystallization of mAb2: mAb2 crystals were grown in batches at the 2.5 mL scale, with each batch yielding about 30 mg of mAb2 in the crystalline form. For each batch, mAb2, PEG buffer, and caffeine buffer were combined at a volume ratio of 3:6:1. Crystallization mixtures were incubated at room temperature for 2 h while rotating at 24 rpm on a rotisserie (Thermo Scientific, model 88881001). mAb2 crystals were recovered from the batches by centrifugation at 1700 RCF for 10 min (Eppendorf MiniSpin Plus), transferred into fresh PEG buffer, resuspended and stored at room temperature for up to 1 week prior to further processing.

Preparation of Prepolymer with mAb2 Crystals: mAb2 crystal suspensions were concentrated through centrifugation at 1700 RCF. The crystal suspension was concentrated up to ≈333 mg mL^{-1} (determined volumetrically) and then diluted to the desired mAb2 concentration by addition of PEG buffer. The prepolymer was prepared by direct addition of PEGDA and Darocur 1173 to the mAb2 crystal suspension, and then vortexed until the mixture was well dispersed.

Microfluidic Formation of Microspheres: Prepolymer droplets were produced with a microfluidic apparatus consisting of two syringe pumps (PHD2000, Harvard Apparatus), a crossjunction (P-891, IDEX; 150 µm orifice), and transparent perfluoroalkoxy alkane tubing (PFA, 1902L, IDEX; OD 1/16", ID 0.001"). Prepolymer was delivered to a single inlet of the crossjunction, and mineral oil was introduced via the two inlets oriented perpendicular to the prepolymer inlet. Droplet formation was controlled by modulating the continuous phase and prepolymer flow rates (Q_C and Q_D, respectively). Droplets were polymerized within the tubing downstream of the crossjunction outlet in a 2" diameter cylindrical enclosure positioned in close contact with a UV LED (M365LP1, Thor Labs; 365nm, 1150 mW). To accommodate higher flow rates, the tubing was coiled several times inside of the enclosure to increase time of exposure. Polymerized droplets were collected in a flask located downstream from the UV LED. Particles were produced with diameters ranging from 30–200 µm. Excess mineral oil was removed from particle suspensions, and then samples were washed in fresh PEG buffer by vortexing for 30 s and centrifugation at 2000 RCF for 2 min at least 4 times to remove residual mineral oil and unreacted hydrogel formers.

For flow curve measurements, suspensions of crystal-loaded hydrogel microspheres were centrifuged at 1700 RCF to increase the nominal volume fraction to reach the target mAb2 loading.

mAb2 Loading and Encapsulation Efficiency: mAb2 content of hydrogels was measured using thermogravimetric analysis (Q500, TA Instruments). Approximately 5 mg of a microsphere suspension was transferred to sampling trays. Excess solvent was wicked from the samples, and they were further dehydrated at 100 °C under 25 mL min^{-1} N_2 flow for 10 min prior to measurement. Samples were heated from 100 to 500 °C, followed by an isothermal hold at 500 °C for 10 min. Sample mass was recorded continuously throughout the experiment from which drug loading and encapsulation efficiency were calculated as described in the Supporting Information. The experiments were performed in triplicate with a 10 °C min^{-1} temperature increase.

Microscopic Characterization of Microspheres: Particle size distribution was evaluated using a Zeiss Axiovert microscope. A minimum of 30 particles were measured (ImageJ) for each sample for each reported mean diameter and coefficient of variation.

Second-order non-linear imaging of chiral crystals (SONICC, Formulatrix) was utilized to collect micrographs of microsphere samples in the following modes: bright-field, ultraviolet two-photon excited fluorescence (UV-TPEF), and SHG.

In vitro Dissolution: Microsphere samples were immersed in 1 mL of PBS and incubated on a rotisserie mixer at 24 rpm. At each sampling interval, the sample was centrifuged for 2 min at 1700 RCF and 0.5 mL of the supernatant was withdrawn and stored at 4 °C until analysis. 0.5 mL of fresh PBS was added to the dissolution sample and it was returned to the rotisserie. Concentration was determined by the Bradford method.

Rheometry: Flow curves were measured using a DHR-3 rheometer (TA Instruments) with a steel parallel plate geometry (40 mm). A parallel plate was used to accommodate microspheres which are incompatible with a cone-plate geometry due to the small truncation length. The gap size was set to 0.25 mm, and >0.35 mL of sample was loaded for each measurement. The rheometer was operated with constant angular velocity and equilibrated for 20 s at each point. A correction was applied to account for the effect of inhomogeneous shear stress on non-Newtonian samples as detailed in the Supporting Information.[50] In the shear rate range tested (up to 4000 s^{-1}), all reported values are above the instrument's torque resolution and below shear rates at which effects of inertia and secondary flows become an issue.[51]

UPSEC: UPSEC was performed on a Waters Acquity UPLC system using a Waters BEH200 SEC column (4.6 × 150mm, 1.7µm) according to the method described previously[52] with modified mobile phase consisting of 50mM phosphate and 450mM Arginine HCl, pH7.0. The sampler temperature was 5 °C, the column temperature was 30 °C. Typically, 30 µg of sample was injected and run for 5 min at a flow rate of 0.5 mL min^{-1}. The elution was monitored by UV absorbance at 280 nm.

Bioassay: The mAb2 competitive binding ELISA evaluated the ability of mAb2 to compete with PD-L1 ligand for binding to PD-1/Fc immobilized on an ELISA plate. The mAb2 reference material and test samples were serially diluted and mixed with an equal volume of rhB7-H1/Fc chimera (PDL-1) dilution before transfer to ELISA plates. The levels of PD-L1 bound to PD-1/Fc are detected by biotinylated anti PDL-1, following conjugation with streptavidin and chemiluminescence substrate. Luminescence was measured using a microplate reader and resulting inhibition response curves were analyzed with curve fitting software (e.g., SoftMax Pro). The IC50 values generated from this assay were a measurement of the ability of mAb2 to inhibit PD-L1 binding to PD-1/Fc. Biological potency was expressed as % relative potency of mAb2 reference material. Geometric mean of relative potency from multiple replicates (N = 3) of the same sample is reported in Table S5, Supporting Information with geometric standard deviation (%GSD) and 95% confidence interval values.

Statistical Analysis: All data were represented as means. Unless otherwise noted, all error bars represent standard deviation of the measurements. Particle sizes were measured with a minimum sample size of 30 particles. Rheological flow curves were measured in duplicate. TGA, dissolution, and ELISA data were collected in triplicate.

Supporting Information

Supporting Information is available from the Wiley Online Library or from the author.

Acknowledgements

The authors acknowledge Merck & Co. Inc. for financial support of the work. The authors also acknowledge Denarra Simmons (Merck & Co.) for supporting the potency study.

 © 2021 Wiley-VCH GmbH

Conflict of Interest

P.R., C.N.N., and X.Y. are Merck & Co. Inc. employees. The authors have filed a patent application based on the results in this article.

Keywords

drug formulations, high concentration, microparticles, protein crystals, suspension rheology

Received: September 29, 2020
Revised: December 23, 2020
Published online:

[1] G. J. Weiner, *Nat. Rev. Cancer* **2015**, *15*, 361.
[2] A. C. Chan, P. J. Carter, *Nat. Rev. Immunol.* **2010**, *10*, 301.
[3] D. Leveque, *Anticancer Res* **2014**, *34*, 1579.
[4] J. Jezek, M. Rides, B. Derham, J. Moore, E. Cerasoli, R. Simler, B. Perez-Ramirez, *Adv. Drug Deliv. Rev.* **2011**, *63*, 1107.
[5] D. S. Tomar, S. Kumar, S. K. Singh, S. Goswami, L. Li, *MAbs* **2016**, *8*, 216.
[6] S. J. Shire, Z. Shahrokh, J. Liu, *J. Pharm. Sci.* **2004**, *93*, 1390.
[7] B. Shenoy, Y. Wang, W. Shan, A. L. Margolin, *Biotechnol. Bioeng.* **2001**, *73*, 358.
[8] P. Garidel, A. B. Kuhn, L. V. Schäfer, A. R. Karow-zwick, M. Blech, *Eur. J. Pharm. Biopharm.* **2017**, *119*, 353.
[9] M. X. Yang, B. Shenoy, M. Disttler, R. Patel, M. McGrath, S. Pechenov, A. L. Margolin, *Sci.* **2003**, *100*, 6934.
[10] R. D. Lawrence, W. Oakley, *BMJ* **1953**, *1*, 242.
[11] B. Reid, M. Gibson, A. Singh, J. Taube, C. Furlong, J. Elisseeff, M. Murcia, J. Elisseeff, *J. Tissue Eng. Regen. Med.* **2015**, *9*, 315.
[12] A. D. Lynn, T. R. Kyriakides, S. J. Bryant, *J. Biomed. Mater. Res. Part A* **2009**, *93A*, 941.
[13] G. M. Cruise, D. S. Scharp, J. A. Hubbell, *Biomaterials* **1998**, *19*, 1287.
[14] K. Pal, B. Behera, S. Roy, S. Sekhar Ray, G. Thakur, *Soft Mater* **2013**, *11*, 125.
[15] E. F. dos Reis, F. S. Campos, A. P. Lage, R. C. Leite, L. G. Heneine, W. L. Vasconcelos, Z. I. P. Lobato, H. S. Mansur, *Mater. Res.* **2006**, *9*, 185.
[16] A. D. Augst, H. J. Kong, D. J. Mooney, *Macromol. Biosci.* **2006**, *6*, 623.
[17] A. Bertz, S. Wöhl-Bruhn, S. Miethe, B. Tiersch, J. Koetz, M. Hust, H. Bunjes, H. Menzel, *J. Biotechnol.* **2013**, *163*, 243.
[18] A. S. Sawhney, C. P. Pathak, J. A. Hubbell, *Macromolecules* **1993**, *26*, 581.
[19] D. Sivakumaran, D. Maitland, T. Hoare, *Biomacromolecules* **2011**, *12*, 4112.
[20] A. Z. M. Badruddoza, P. D. Godfrin, A. S. Myerson, B. L. Trout, P. S. Doyle, *Adv. Healthc. Mater.* **2016**, *5*, 1960.
[21] P. D. Godfrin, H. Lee, J. H. Lee, P. S. Doyle, *Small* **2019**, *15*, 1803372.
[22] S. Kirchhof, M. Gregoritza, V. Messmann, N. Hammer, A. M. Goepferich, F. P. Brandl, *Eur. J. Pharm. Biopharm.* **2015**, *96*, 217.
[23] S. P. Zustiak, J. B. Leach, *Biotechnol. Bioeng.* **2011**, *108*, 197.
[24] J. E. Mealy, J. J. Chung, H. H. Jeong, D. Issadore, D. Lee, P. Atluri, J. A. Burdick, *Adv. Mater.* **2018**, *30*, 1705912.
[25] A. C. Daly, L. Riley, T. Segura, J. A. Burdick, *Nat. Rev. Mater.* **2020**, *5*, 20.
[26] H. M. Shewan, J. R. Stokes, *J. Colloid Interface Sci.* **2015**, *442*, 75.
[27] P. Panda, S. Ali, E. Lo, B. G. Chung, T. A. Hatton, A. Khademhosseini, P. S. Doyle, *Lab Chip* **2008**, *8*, 1056.
[28] J. L. West, J. A. Hubbell, *React. Polym.* **1995**, *25*, 139.
[29] A. G. Lee, C. P. Arena, D. J. Beebe, S. P. Palecek, *Biomacromolecules* **2010**, *11*, 3316.
[30] N. W. Choi, J. Kim, S. C. Chapin, T. Duong, E. Donohue, P. Pandey, W. Broom, W. A. Hill, P. S. Doyle, *Anal. Chem.* **2012**, *84*, 9370.
[31] P. Wu, Y. Wang, Z. Luo, Y. Li, M. Li, L. He, *Lab Chip* **2014**, *14*, 795.
[32] E. Amstad, M. Chemama, M. Eggersdorfer, L. R. Arriaga, M. P. Brenner, D. A. Weitz, *Lab Chip* **2016**, *16*, 4163.
[33] E. Stolovicki, R. Ziblat, D. A. Weitz, *Lab Chip* **2018**, *18*, 132.
[34] Telos High-Throughput Systems, https://www.dolomite-microfluidics.com/microfluidic-systems/telos-high-throughput (accessed: December 14, 2020).
[35] L. M. Weber, C. G. Lopez, K. S. Anseth, *J. Biomed. Mater. Res. Part A* **2008**, *90A*, 720.
[36] M. B. Mellott, K. Searcy, M. V. Pishko, *Biomaterials* **2001**, *22*, 929.
[37] G. Jahanmir, C. M. L. Lau, M. J. Abdekhodaie, Y. Chau, *ACS Appl. Bio Mater.* **2020**, *3*, 4208 .
[38] D. Dendukuri, P. Panda, R. Haghgooie, J. M. Kim, T. A. Hatton, P. S. Doyle, *Macromolecules* **2008**, *41*, 8547.
[39] X. Huang, C. S. Brazel, *J. Control. Release* **2001**, *73*, 121.
[40] L. L. Wright, A. G. Palmer, N. L. Thompson, *Biophys. J.* **1988**, *54*, 463.
[41] S. P. Meeker, R. T. Bonnecaze, M. Cloitre, *J. Rheol.* **2004**, *48*, 1295.
[42] I. E. Zarraga, R. Taing, J. Zarzar, J. Luoma, J. Hsiung, A. Patel, F. Lim, *J. Pharm. Sci.* **2013**, *102*, 2538.
[43] J. A. Pathak, R. R. Sologuren, R. Narwal, *Biophys. J.* **2013**, *104*, 913.
[44] R. A. Chilton, R. Stainsby, *J. Hydraul. Eng.* **1998**, *124*, 522.
[45] H. L. Hernandez, J. W. Souza, E. A. Appel, *Macromol. Biosci.* **2020**, 2000295.
[46] T. E. Robinson, E. A. B. Hughes, A. Bose, E. A. Cornish, J. Y. Teo, N. M. Eisenstein, L. M. Grover, S. C. Cox, *Adv. Healthc. Mater.* **2020**, *9*, 1901521.
[47] M. Syedbasha, J. Linnik, D. Santer, D. O'Shea, K. Barakat, M. Joyce, N. Khanna, D. Lorne Tyrrell, M. Houghton, A. Egli, *J. Vis. Exp.* **2016**, *2016*, e53575.
[48] J. Li, D. J. Mooney, *Nat. Rev. Mater.* **2016**, *1*, 16071.
[49] D. K. Hwang, J. Oakey, M. Toner, J. A. Arthur, K. S. Anseth, S. Lee, A. Zeiger, K. J. Van Vliet, P. S. Doyle, *J. Am. Chem. Soc.* **2009**, *131*, 4499.
[50] J. F. Steffe, *Rheological Methods in Food Process Engineering*, 2nd ed., Freeman Press, East Lansing **1996**.
[51] R. H. Ewoldt, M. T. Johnston, L. M. Caretta, in *Complex Fluids in Biological Systems* (Ed: S. Spagnolie), Springer Biological Engineering Series, Springer, Berlin **2015**, pp. 207–241.
[52] X. Mou, X. Yang, H. Li, A. Ambrogelly, D. J. Pollard, *Pharm. Bioprocess.* **2014**, *2*, 141.

 © 2021 Wiley-VCH GmbH